Subwavelength porous silica antireflection coating

X. YE, J. HUANG, J. C. ZHANG, X. D. JIANG*, W. D. WU, W. G. ZHENG
Research Center of Laser Fusion, CAEP, P. O. Box 919-987, MianYang 621900, China

A non-close packed polycrystalline colloidal crystal for antireflection (AR) coating was fabricated on transparent substrate by dip coating method. Self assembled polycrystalline colloidal crystals were used as a nanometer scale composite material with controlled thickness and low refractive index. It can turn the max-transmission wavelength from visible light to infrared wave with different withdraw velocities prepared coatings. The novel microstructures have relatively high laser-induced-damage thresholds. A series of films with different structures were fabricated by changing the preparation parameters. The results suggest that the thickness of coatings determines the max-transmission wavelength and the fill factor of nanometer particles exert an influence on the transmission efficiency. The research results indicate that the max-transmission efficiency through the transparent substrate with sub-wavelength porous silica coating is increased to 99.8%. Scanning electron microscope (SEM) was used to characterize the surface morphology of porous silica coatings. And the AR coatings exhibit broadband enhanced transmission. The Nd:YAG laser damage threshold of the as-prepared reflection reducing coatings is about 21.74 J/cm^2 at 1064 nm. The environmental durability of subwavelength AR microstructures was investigated with promising initial results reported.

(Received April 5, 2011; accepted May 25, 2011)

Keywords: Subwavelength, Porous, Antireflective Coatings, Effective Medium Theory, Laser-Induced-Damage Thresholds

1. Introduction

The decrease in transmission of a transparent optical medium is mainly caused by the abrupt change in the refractive index at the interface between a medium and its environment. One characteristic of a desirable optical material is the low refractive index. Antireflection (AR) coatings reduce the reflection considerably improving the quality of optical systems. In designing an antireflection coating we require low refractive indices of the film to match those of various substrates [1]. In spite of intensive research, the availability of antireflection coatings is still limited by lack of materials with low refractive indices. The refractive indices of glass and transparent plastic substrates are typically $n_s \approx 1.5$. The optimal refractive index for a single-layer antireflection coating is $n_f = \sqrt{n_s} \approx 1.22$. The lowest refractive indices for the dielectrics are about 1.35 (CaF_2, MgF_2). A value of n_f = 1.22 is therefore unreachable for conventional single layer AR coatings [2]. Optical nanostructures are one type of composite materials with low refractive indices. These materials typically consist of various fractions of air and a base material, and the nanostructures could be equivalent to a single-layer AR coating for equation medium theory (EMT), as the feature size is less for visible wavelength [3~5]. Such a feature size is beyond the conventional photolithography capability. Besides, electron beam lithography, X-ray lithography, scanning tunneling microscopy, and atomic force microscopy lithography are alternative methods. Although they have abilities to create the nanostructure, they cannot be afforded by most laboratories because of their high costs and low sample throughout [6]. Recently, some researches have developed some other strategies mainly on self-assembly processes. One of these routes, the 2D colloidal crystals has been used for AR coatings. But the optical coating material is polystyrene (PS), loading to low laser-induced-damage thresholds (LIDT) [7]. And obviously this method is not suitable for adjusting reflective index and thickness of thin film. In this letter we report a simple and effective method for creating nanoscale optical composite materials by using non-close packed polycrystalline colloidal crystal on a substrate. We demonstrate the preparation of the nanoporous AR coatings with microstructure on glass substrates by dip-coating technique and showing the dependence of variation of the AR behaviour on different deposition process parameters and particle volume frication. The laser damage threshold of AR coating were carried out on Nd:YAG lasers at l064nm (1H).

2. Experimental

2.1 Synthesis of silica particles

Silica particles was prepared by the Stober process [8].In a 500ml conical flask, a mixture containing 1.8M $NH_3.H_2O$ (25%~28.0% NH_3 solution in water), 0.2M Tetraethoxysilane (TEOS was vacuum distilled before use for particle synthesis.), 2M H_2O and 85vol% ethanol was stirred at 55^{o}C temperature for 10h. The resulting silica suspension was centrifuged at 10000rmp for 1 hour and washed by repeating redispersion three times in pure

ethanol and three times in deionized water. The diameter of the silica spheres was determined by scanning electron microscopy (SEM). The mean diameter of the particles was 89 nm.

2.2 Formation of 2D array of particle by dip-coating

Experimental procedures are as follows: First, a suspension of the particles was diluted to a definite concentration using ethanol. Then a hydrophilic glass substrate was immersed vertically into the dispersion and lifted up with a constant speed, which was precisely controlled by a motor. The temperature for the experiment was at 25 ℃.

2.3 LIDT measurements

The LIDT was test with the route shown in Fig. 2. A Q-tuned Nd:YAG laser was used to provide a near-Gauss-type pulse beam (spatially and temporally) at a 1064 nm wavelength. A fixed energy attenuator was installed in the beam path to provide energy control. The maximum output energy was up to 800mJ. The diameter of the laser spot on the testing film was ~740um (the width at $1/e^2$ of the pulse intensity), and the pulse width was ~3ns. The R-on-1 testing procedure was carried out at 20 locations that were arranged in to a 4×5 array. According to ISO11145, the distance between any two closer irradiated spots was 5mm, which was long enough to avoid the over lapping of damage regions. By increasing the energy irradiated on the film at an increment of 0.3mJ and a time interval of 3s, the films were shot until breakdown damage (plasma flash) occurred, and this energy was recorded at once. The final LIDT of film and substrate were the root mean square of 20 breakdown damage energies.

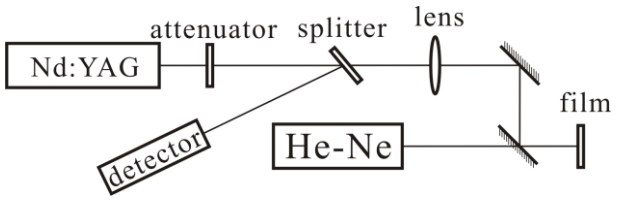

Fig. 1. Schematic of the testing optic of laser-induced threshold.

2.4 Stability measurements

A process for fabricating random distribution AR microstructures directly in the surface of K9 glass has been developed. One application of this microstructure is for vacuum. To evaluate the environmental durability of the subwavelength porous AR coating and sol gel AR coating K9 glass for vacuum application, a 40×40mm K9 glass was subjected to a vacuum of 10^{-3} Pa with silicone oil using a environmental test chamber.

3. Results and discussion

3.1 Non-close packed polycrystalline colloidal crystals structures

Dip-coating is the most popular method in which the colloids are evaporation induced and self-assembled on the substrate as it slowly withdrawn from the colloidal suspension. When the substrate is drawn from the silica emulsion, a meniscus region can be formed on the substrate due to the wetting from the solution, which leads to the accumulation of silica particles by the viscous drag upward on the liquid by the moving substrate and lateral capillary forces.

Fig. 2 shows SEM images of the subwavelength porous AR coating and sol gel AR coating [9]. Fig. 2a shows subwavelength porous AR films consist of non-closely packed silica fine particles. In Fig.2b, Side-view SEM image of the sol-gel layers are shown. SEM images (Fig.2b) revealed a homogeneous distribution of the pores inside the sol-gel coating.

To get the fill factor of the structure, which is the volume percentage of the nanoparticles in the film, we used image processing method, morphological operation, and watershed region segmentation method to calculate the number of particles and to verify the mean diameter of the silica nanoparticles. The calculated value of fill factor was 0.4487 (Fig. 2(a).

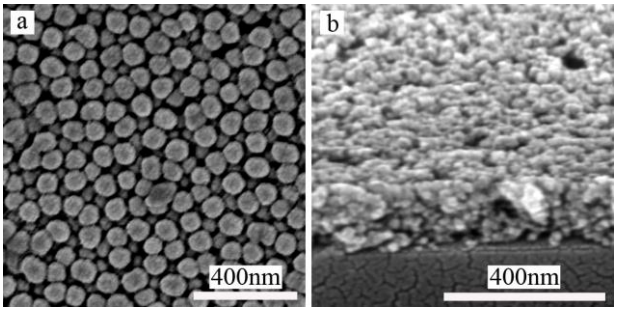

Fig. 2. SEM images of subwavelength porous AR coating and sol gel AR coating: (a) subwavelength porous AR coating, (b) sol gel AR coating [9]

3.2 Optical properties

The reflection loss of an optical surface is related to the difference between the refractive indices of film and the optical material. The optimal refractive index for a single-layer antireflection coating is $n_f = \sqrt{n_s \cdot n_{air}} \approx 1.22$. When the structure feature size is much lower than the

wavelength, the effective reflective index can be approximated by $N = \sqrt{n_f^2 \cdot f + n_{air}^2 \cdot (1-f)} \approx 1.22$, based on the "effective medium theory" (EMT). Where n_f is the refractive index of silica nanoparticles, n_{air} is the refractive index of air, and f is the fill factor.

In general, some interdependent factors can play a role in the final optical properties of the coating: (i) silica concentration; (ii) withdraw velocity. In our investigations, the different rate of dip-coating was used (50mm/min~400min). And the solutions with final silica concentration of 1.41(m)%, 2.04(m)%, 2.55(m)%, 3.4(m)%, and 4.07(m)% SiO_2 were prepared. Several different concentrations were used and studied in an effort to find the optimal deposition conditions on the K9 glass for antireflective behavior. The transmission spectra of silica coating obtained on the glass substrate using different concentration of SiO_2 and deposition rate were recorded. The variation of AR behavior for different coatings on K9 obtained from 1.41(m)%, 2.04(m)%, 2.55(m)%, 3.4(m)%, and 4.07(m)% SiO_2 solution are shown in Figs. 3~7, respectively.

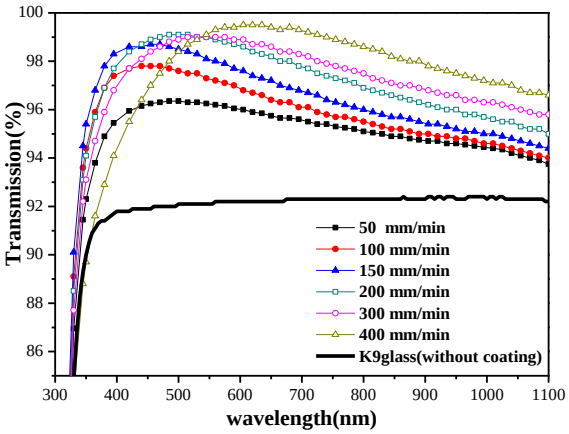

Fig. 3 Transmission spectra for silica coating glass obtained from 1.41(m)% SiO_2 using different deposition rate.

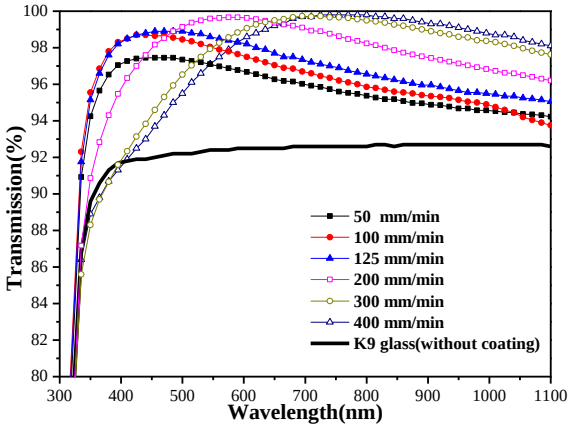

Fig. 4. Transmission spectra for silica coating glass obtained from 2.04(m)% SiO_2 using different deposition rate

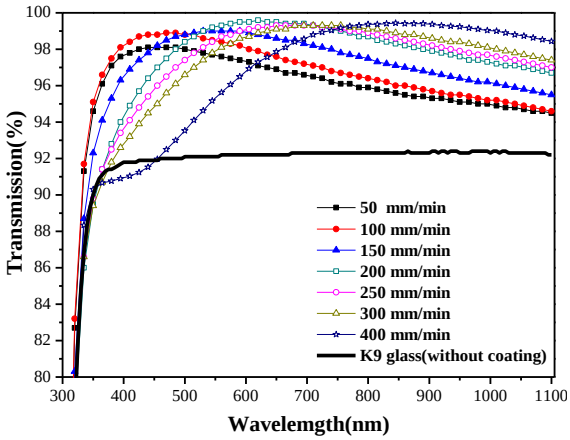

Fig. 5 Transmission spectra for silica coating glass obtained from 2.55(m)% SiO_2 using different deposition rate.

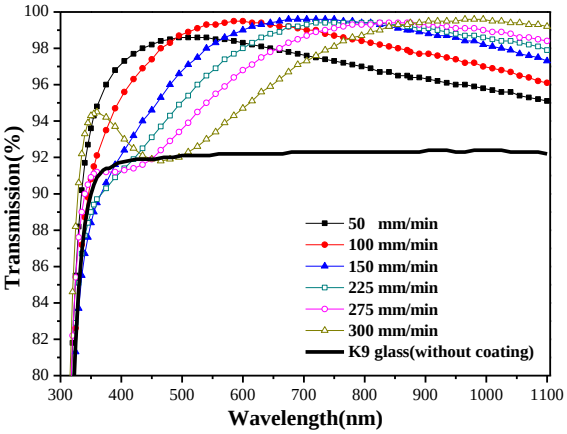

Fig. 6. Transmission spectra for silica coating glass obtained from 3.4(m)% SiO_2 using different deposition rate.

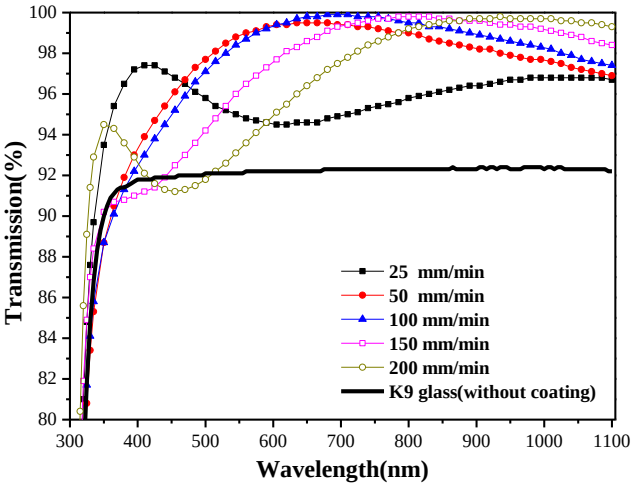

Fig. 7. Transmission spectra for silica coating glass obtained from 4.07(m)% SiO_2 using different deposition rates.

It is evident that in all cases the coating visibly reduced the reflectance of the K9 glass. As seen, the transmission spectra show a sinusoidal shape with a single maximum if the quarter-wave thickness occurred over the wavelength. Such behaviour is typical and expected for the single layer coating. The data collected for the different deposition rates showed the precise tuning of the spectral maxima. The relative difference in spectral behaviour for different rates is caused mostly by variation of film thickness [10]. The observed shift in the transmission maxima correlates very well with the deposition rate, proving that the optical properties of the coating can be controllably varied by the deposition process. As seen from Fig. 3, the transmission maximum for both sided coating obtained from 1.41m%, 400mm/min on glass was found to be 99% occurred in the wavelength of 600nm. However, there are non-uniform surface on the coating when withdraw velocity is higher. It's evident that from the Fig. 3~7 the transmission maximum is shifted from the short wavelength to the longer wavelength with increasing the immersing rate. The maximum transmission for a both coating was found to be about 99.8% (see Fig. 3~7). At the higher concentration, the optimal coating is exhibited (Fig. 5~7). The results can be rationalized in terms of reason as follows: (i) it can turn the max-transmission wavelength from visible light to infrared wave by different withdraw velocity simply. (ii) The large scale uniform coating for lower deposition rate is caused mostly by higher concentration; e.g. the maximum transmission for a both sided coating obtained from 1.41m% SiO2 solution, 400mm/min on glass was 600nm wavelength. However, the coating deposited at 4.07m% SiO2 solution, 50mm/min showed the best antireflective properties in the 600nm wavelength. (iii) The coatings obtained from higher concentration exhibit broadband antireflective properties, e.g. the broadband of transmission efficiency above 99% reach 300nm (seen Fig. 5~7).

The maximum transmission for a coating obtained from 1.41m% SiO_2 emulsion was found to be about 96.3%~99.1% (see Fig. 3). As seen from Fig. 3, the intensity of transmission increases with increasing the immersing rate from 50mm/min (96.3%) to 200mm/min (99.1%). The changes of refractive index of the coating resulted in the changes of antireflective properties.

Five colloidal SiO_2 of the different concentration (1.41(m)%, 2.04(m)%, 2.55(m)%, 3.4(m)%, and 4.07(m)%) were selected to study the influence of concentration on the transmittance (Fig. 8). The thickness of AR coating increases with increasing silica concentration of the emulsion of silica particles; as consequence, the transmission maximum is shifted from 450nm to longer wavelength.

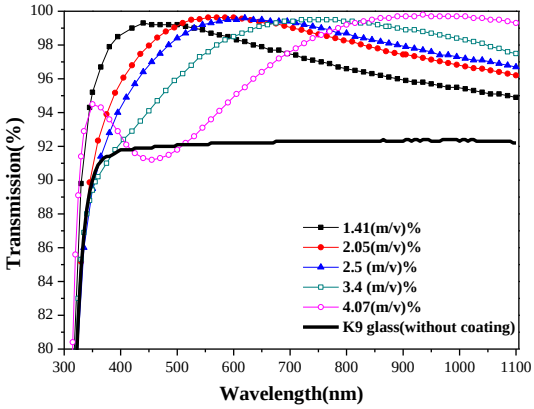

Fig. 8 Transmission spectra for silica coating on glass substrates obtained from different concentration SiO2 solution. The dipping rate was 200mm/min.

3.3 LIDT of Coating

It is so important for ICF engineering that property of silica antireflective films have the high laser damage threshold [11~13]. The laser damage threshold of fused silica with AR coating exceeded 21.74 J/cm^2 we found that the LIDT of the AR coating was much approaching to the fused silica without the AR coating (22.74 J/cm^2).

3.4 Stability and life of AR coating

The curve in Fig. 9 shows the transmission of the AR coating of the tests. Note the greater than 99.5% transmission at 1064nm at the start of the tests. The transmission of the subwavelength AR coating has decreased by less than 2% after 15 days of exposure. However, the peak transmittance of the sol-gel AR coating decreased from 100% to 95% under the same condition. The porous microstructure can influence the environmental durability because of adsorbing volatile organic compounds. The subwavelength porous AR coatings excel sol gel AR coatings in vacuum organic contamination resistant property.

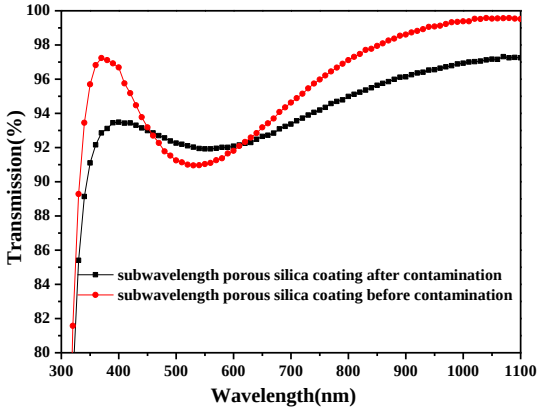

Fig. 9 Measured transmission of a K9 glass with subwavelength porous AR textures fabricated in both surfaces. The transmission was measured before and after 15 day exposures to vacuum.

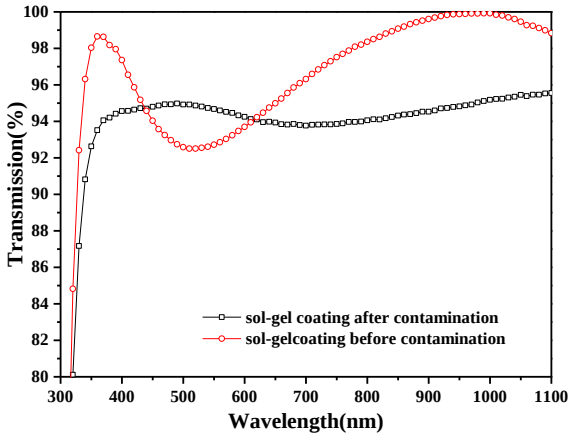

Fig.10. Measured transmission of a K9 glass with sol-gel ARcoating fabricated in both surfaces. The transmission was measured before and after 15 day exposures to vacuum.

4. Conclusions

The optical properties and microstructure of sub-wavelength porous silica AR coatings deposited by dip-coating technique were characterized in detail in this study. The formation of silica antireflective coatings by changing preparation parameters has been investigated. We found that using optimal deposition parameter (drawing rate or concentration of silica) the AR coating can approach maximum transmission 99.8%. It can turn the max-transmission wavelength from visible light to infrared wave (400nm~1100nm) by different withdraw velocity. The AR coating exhibit broadband antireflection properties; e.g. the broadband of transmission efficiency above 99% exceed 300nm. The Nd:YAG laser damage threshold of reflection reducing coating exceeded 21.74 J/cm^2 at 1064 nm. The results also show that the stability and life of subwavelength porous AR coating are improved. Subwavelength AR structures offer the potential for low cost fabrication through simplified processing requirements and through high volume replication techniques.

Acknowledgments

This work was supported by the National Natural Science Foundation of China (NSFC 60908023).

References

[1] D.G. Chen, Solar Energy Materials & Solar Cells, **68**, 313 (2001).
[2] Y. X. Cui, L. Zhang, Y. Xu, D. Wu, H. B. Lv, H. J. Wang, X. D. Jiang, High Power Laser and Particle Beams **20**, 401 (2008).
[3] E. B. Grann, M. G. Moharam, D. A. Pommet, J. Opt. Soc. Am. A, **12**, 333 (1995).
[4] D. W. Zhang, Z. W. Lu, W. X. Yu., F. Y. Li, Chinese Journal of Lasers, **B11**, 273 (2002).
[5] P. B. Clapham, M. C. Hutley, Nature **244**, 281 (1973).
[6] Y. Li, W. P. Cai, G. T. Duan, Chem. Mater **20**, 615 (2008).
[7] Y. Zhao, J. S. Wang, G. Z. Mao, Opt. Lett, **30**, 1885 (2005).
[8] G. H. Bogush, M. A. Tracy, C. F. Zukoskiiv, Journal of Non-Crystalline Solids **104**, 95 (1988).
[9] L. H. Yan, X. D. Jiang, B. Jiang, X. D. Yuan, H. B. Lv, High Power Laser and Particle Beams, **19**, 767 (2007).
[10] L. J. Crawford, N. R. Edmonds, Thin Solid Films, **515**, 907 (2006).
[11] Y. Xu, L. Zhang, D. Wu, Y. H. Sun, Z. X. Huang, X. D. Jiang, X. F. Wei, Z. H. Li, B. Z. Dong, Z. H. Wu, J. Opt. Soc. Am. B **22**, 905 (2005)
[12] Y. Xu, L. Zhang, D. Wu, Y. H. Sun, Z. X. Huang, X. D. Jiang, X. F. Wei, Z. H. Li, B. Z. Dong, Z. H. Wu, J. Opt. Soc. Am. B, **22**, 1899 (2005).
[13] Y. J. Guo, X. T. Zu, X. D. Jiang, X. D. Yuan, S. N. Zhao, S. Z. Xu, B. Y. Wang, D. B. Tian, High Power Laser and Particle Beams, **20**, 939 (2008).

* Corresponding author: yehanwin@mail.ustc.edu.cn,